JACS
JOURNAL OF THE AMERICAN CHEMICAL SOCIETY

ARTICLE

pubs.acs.org/JACS

Mechanistic Insights into Heterogeneous Zinc Dicarboxylates and Theoretical Considerations for CO_2−Epoxide Copolymerization

Stephan Klaus,[†] Maximilian W. Lehenmeier,[†] Eberhardt Herdtweck,[‡] Peter Deglmann,[§] Anna K. Ott,[§] and Bernhard Rieger*[,†]

[†]WACKER-Lehrstuhl für Makromolekulare Chemie and [‡]Anorganisch-Chemisches Institut, Technische Universität München, Lichtenbergstrasse 4, 85747 Garching bei München, Germany

[§]BASF SE, GKT - B001 67056 Ludwigshafen, Germany

Supporting Information

ABSTRACT: Copolymerization of epoxides and CO_2 with heterogeneous zinc dicarboxylates is prominent since the early days of this area of chemistry. However, in over 30 years of research, the efficiency of this catalyst system could not be improved significantly. Furthermore, a huge activity difference between zinc glutarate and its lower homologue zinc succinate exists, which could not be explained so far. A detailed investigation of the underlying copolymerization mechanisms on heterogeneous catalysts is therefore necessary. Such investigations are so far lacking, which renders logical improvements of the catalysts difficult. We therefore decided to conduct a detailed investigation on the different zinc-dicarboxylic catalysts, their copolymerization efficiency, solid state structure and supplemented the results with theoretical calculations. The results imply that the widely discussed bimetallic mechanism (for homogeneous catalysts) is in place for heterogeneous zinc dicarboxylates as well. Theoretical calculations conducted to identify an "ideal" Zn−Zn distance suggest an optimal separation of Zn atoms in the range of 4.3−5.0 Å. The combined copolymerization experiments and calculated models give a consistent explanation for the difference in activity of the different zinc-dicarboxylate catalysts and give a hint why the activity of the heterogeneous zinc-dicarboxylate system is limited.

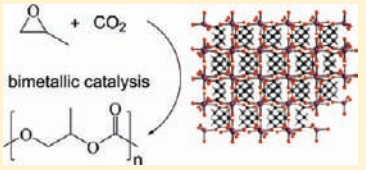

INTRODUCTION

As crude oil sources will perish in a foreseeable future, the interest in alternative and renewable sources for raw materials is increasingly gathering the focus of global research activities.[1−4] One such source is CO_2, which is released in many combustion processes and is, besides methane, considered as a main origin of the unpopular greenhouse effect.[5−8] Utilization of CO_2 as C_1-feedstock for copolymerization reactions would help to slightly reduce the atmospheric CO_2-content by simultaneously delivering high-valor polymeric products.[9−12]

The copolymerization of CO_2 with epoxides is known since 1969, when Inoue et al. combined diethylzinc, water, CO_2, and propylene oxide to yield polymer in low yields.[13] This initial experiment was followed by innumerable consecutive works, which all had to struggle with low catalytic activities and undesired side products like cyclic carbonate or high contents of ether linkages in the polymer (Scheme 1).

Although contrary hypothesis exist on the initiation and propagation mechanism of alternating CO_2/epoxide copolymerization, recent publications mostly consider homogeneous systems to work in a cooperative (binary or bimetallic) pathway.

One of the first investigated catalysts to prove the bimetallic mechanism were the β-diiminate (BDI) complexes, which are most active in their dimeric state.[14−16] At very low concentration, the monomer−dimer equilibrium is shifted to the monomeric side and almost no catalytic activity is observed.[17,18] At higher concentrations, BDI-complexes are found in their dimeric state,

Scheme 1. Alternating Copolymerization of CO_2 and PO and Side-Product Pathways: Formation of Cyclic Carbonate through Backbiting and Polyether Formation through Consecutive PO Insertions

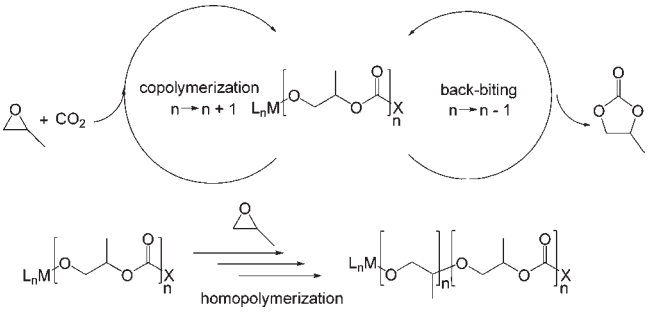

in which two metal sites spatially come close to each other, allowing them to interact and form the respective polycarbonate.

The cooperative behavior of different catalysts has extensively been summarized in several recent reviews.[19−21] In a theoretical study conducted by us, we predicted chain growth to take place via the attack of a metal-bound alkyl carbonate on a metal-coordinated epoxide.[22] Such a bimolecular process has also been observed by Jacobsen et al. for the asymmetric ring-opening of

Received: May 23, 2011
Published: July 11, 2011

Scheme 2. Bimetallic Reaction Pathway for CO_2/PO Copolymerization on Zinc Dicarboxylate Surface

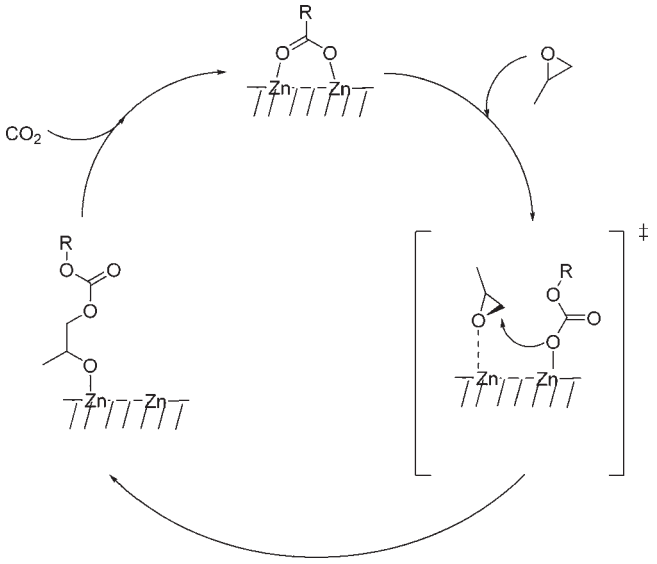

epoxides.[23−25] Also others have reported a bimetallic initiation, which to their believe is followed by a monometallic propagation step.[26−29] These considerations led to the design and application of well-defined, rigid dinuclear complexes[17,30−37] and flexibly linked salen-type complexes in recent years.[38,39]

In this work, we suppose the heterogeneous zinc-dicarboxylates to copolymerize in a bimetallic fashion as well. The bimetallic reaction pathway involves the interaction of two active sites on the surface of a zinc dicarboxylate (Scheme 2). The copolymerization proceeds by two iteratively alternating reactions: (i) CO_2 insertion into a zinc−alkoxide bond; (ii) nucleophilic attack of a precoordinated epoxide by a carbonate.

Copolymerization mechanisms on heterogeneous catalysts and especially zinc dicarboxylates have not been reported so far. The copolymerization of epoxides and CO_2 with heterogeneous zinc glutarate is prominent since the early days of this area of chemistry. However, in over 30 years of research, the efficiency of this system could not be improved significantly. Furthermore, a huge activity difference between zinc glutarate and its lower homologue zinc succinate exists, which could not been explained so far. The composition of such heterogeneous catalysts is often ambiguous and the active sites are generally only poorly defined which renders logical improvements of the zinc dicarboxylates difficult. Nonetheless, zinc dicarboxylates are industrially employed for the production of polycarbonates and the majority of commercial PPC is produced with the use of zinc glutarate.

The zinc glutarate (ZnGA) comprising Zn and glutaric acid is the most intensively studied system. The molecular structure of ZnGA has only recently been resolved and shows a unique structure type, where four carboxyl groups coordinate one Zn center.[40,41] The glutarate ligands are found in either a bent or an extended conformation (Figure 3B). This leads to the formation of two metallacycles A and B that introduce a porosity which is not conclusive for monomer diffusion.[42] These investigations showed that overall activity is restricted to the outer surface of the ZnGA-particles.

Initial strategies to increase the activity were therefore focused on increasing the ZnGA surface area by one of four methods (stirring procedure, post-modification, additives, growth controllers).[43,44] Each of these strategies has been tested in literature and shown to enhance activity, although the desired high activities that have been realized for several homogeneous catalysts have not been achieved with zinc dicarboxylates to date.[42,43,45−48]

Besides the surface area, the crystallinity is often considered as main contributor to the activity. This topic has been discussed ambivalently; however, it seems that amorphous catalysts are less active than their highly crystalline counterparts.[42−44,49−52] This shows how important the material (bulk) and especially the surface constitution on heterogeneous zinc dicarboxylates is for an activity in CO_2/PO copolymerization.

Other attempts to increase catalytic activities were based on the exchange of glutaric acid for its higher or lower homologues. Recent reports have demonstrated that ZnAA (with adipic acid, C_6, TOF = 580 h^{-1})[53,54] and ZnPA (with pimelic acid, C_7, TOF = 530 h^{-1})[52] (all TOF values in $g \cdot mol^{-1} \cdot h^{-1}$) show similar activities to ZnGA when appropriately treated. Adipic acid is of particular interest as this is a large-scale industrial product. Interestingly, the same trend of activity for analogous structures of ZnGA is observed when the functionalization route with $ZnEt_2$, followed by SO_2 activation, is employed. The activity slightly decreases in the order of ZnGA (TOF = 630 h^{-1}) > ZnAA (TOF = 529 h^{-1}) > ZnPA (TOF = 459 h^{-1}); almost no activity is observed for ZnSA (TOF = 7 h^{-1}).[55]

These results indicate that the activity of heterogeneous zinc dicarboxylates of this type is dependent on a defined spatial structure which is influenced by the dicarboxylic acid used. From these catalysts, only the solid state structures of ZnGA[40,41] and ZnSA[56,57] have been reported so far. These two systems have a considerably differing structure, which we believe to be the crucial factor for the inefficiency of ZnSA to copolymerize CO_2 and PO, whereas its higher homologues are able to do so.

To gather a more complete understanding of the surface processes on zinc dicarboxylates, the optimal Zn−Zn distance for copolymerization, and the difference between ZnSA and its higher homologues, we designed a synthesis procedure which allows comparison of all four zinc dicarboxylates (ZnSA, ZnGA, ZnAA, and ZnPA) and their efficiency in CO_2/PO copolymerization. Through careful handling in inert atmosphere, we were able to prove that the surface needs to be activated in order to generate initiator groups that are able to copolymerize.

Moreover, comparison of the solid state structures, surface areas, particle sizes, and copolymerization efficiency allows to deduce a bimetallic mechanism. The results are corroborated by theoretical calculations on molecular model systems, delivering the optimal Zn−Zn distance for copolymerization. This study gives an insight into the long-known heterogeneous zinc dicarboxylates and the underlying mechanism and active species for the alternating copolymerization of CO_2 and epoxides.

EXPERIMENTAL SECTION

Reagents and Methods. All reactions of air- and/or moisture sensitive compounds were performed under an atmosphere of dry argon using standard Schlenk techniques or in an inert atmosphere glovebox. All chemicals were purchased from Aldrich, Acros and ABCR and used as delivered unless stated otherwise. Solvents were obtained from a solvent-purification system MBraun MB-SPS. Propylene oxide was dried over CaH_2 and freshly distilled prior to use. Solution NMR spectra of the polymers were collected at room temperature using a Bruker ARX300 spectrometer. ^1H NMR spectra are referenced to $SiMe_4$ by the residual

solvent peak. The molecular weights were determined with a Varian PL-GPC-50 at 35 °C and the eluent THF. Physisorption measurements to determine the surface area and mesopore size distribution (using nitrogen as inert gas) were performed with a Sorptomatic 1990 instrument (ThermoQuest GmbH, Bremen, Germany). Surface areas were determined according to the BET model. Tunnel electron microscopy pictures were taken with a JEOL JEM 100CX TEM microscope, and scanning electron microscopy pictures were taken with a JEOL JSM 5900 LV SEM microscope.

Synthesis of Standard-ZnGA. ZnGA was synthesized with slight variations as reported elsewhere.[42,43,49,50] In a heated 250 mL Schlenk-vessel with reflux condenser and dean-stark trap, 2.76 g (34.0 mmol) of zinc oxide and 4.49 g (34.0 mmol) of glutaric acid were suspended in 200 mL of toluene. The mixture was heated one day at 80 °C in an inert argon atmosphere. After cooling the reaction mixture, the white precipitate was filtered and washed with acetone, and the product was dried in a vacuum oven at 130 °C, delivering 6.72 g (34 mmol, 100%) of the product as powder. The material was characterized via PXRD, IR, SEM, and TEM and was used in this report as reference system. ZnGA: IR(ATR) (cm^{-1}): 2929, 1536, 1453, 1405, 1354, 829, 763, 677, 559.

Synthesis of Crystalline Zinc Dicarboxylates (Hydrothermal). A total of 2.97 g (10.0 mmol) of zinc nitrate hexahydrate was dissolved together with 10 mmol of the correspondent dicarboxylic acid in 20 mL of water, introduced into a glass-autoclave, and heated to 180 °C in a heating block. After several hours at this temperature, the glass vessel was interstratified with streaks that eventually form the crystalline particles after 1−30 days, depending on the dicarboxylic acid used. The reaction mixture was cooled to room temperature and the white crystalline precipitate was filtered, washed with water and acetone, and dried in a vacuum oven at 130 °C. Even though this procedure generally suffers from low yields, highly crystalline particles can be gathered in all cases. Several of these crystals were collected for structure determination. ZnSA: weighed succinic acid, 1.2 g; reaction time, 4 weeks; yield, 33%. ZnGA: weighed glutaric acid, 1.3 g; reaction time, 2 weeks; yield, 15%. ZnAA: weighed adipic acid, 1.5 g; reaction time, 7 days; yield, 25%. ZnPA: weighed pimelic acid, 1.6 g; reaction time, 3 days; yield, 27%.

Single Crystal X-ray Structure Determinations. *ZnAA.* Colorless fragment, $C_6H_8O_4Zn$, M_r = 209.51; monoclinic, space group $P2/c$ (Nr. 13), a = 16.1050 (12), b = 4.7876 (4), c = 9.2686 (7) Å, β = 90.024 (4)°, V = 714.65 (10) Å^3, Z = 4, λ(Mo Kα) = 0.71073 Å, μ = 3.394 mm^{-1}, ρ_{calcd} = 1.947 g cm^{-3}, T = 123(1) K, F(000) = 424, θ_{max}: 25.34°, R1 = 0.0170 (1297 observed data), wR2 = 0.0437 (all 1306 data), GOF = 1.204, 101 parameters, $\Delta\rho_{max/min}$ = 0.31/−0.27 eÅ^{-3}. CCDC-825764 (**ZnAA**). For more details see Supporting Information.

ZnPA. Colorless plate, $C_7H_{10}O_4Zn$, M_r = 223.54; monoclinic, space group $P2/c$ (Nr. 13), a = 38.008 (3), b = 4.7381 (3), c = 9.2728 (6) Å, β = 91.439 (4)°, V = 1669.4 (2) Å^3, Z = 4, λ(Mo Kα) = 0.71073 Å, ρ_{calcd} = 1.779 g cm^{-3}, T = 123(1) K. Due to an unresolvable disorder of one pimelate anion, the refinements were aborted.

Ball-Milling and Post-Activation. The crystalline particles from the hydrothermal synthesis route were introduced into a planetary ball-mill type PM 100 from Retsch GmbH in an inert argon atmosphere. To minimize abrasion during the grinding procedure, a 50 mL ZrO_2-beaker and ZrO_2-balls (Ø = 2 mm) were used. The ball-milling procedure was conducted for 4 h at 300 rpm. The beaker was rotated into one direction for 10 min and, after a 5-min pause, rotated into the opposite direction for 10 min. This procedure was repeated until the added ball-milling events reached 4 h. Additionally, ZnGA was ball-milled for 10 min, 30 min, 1 h, 2 h, and 4 h in the same manner as previously described. One part of the powder was taken as is for copolymerization, and the rest was activated in a saturated water atmosphere overnight and dried thoroughly in a vacuum oven at 130 °C.

Polymerization Experiments. All polymerization experiments were performed in 100 mL steel autoclaves equipped with magnetic stirring and oil bath heating. The autoclaves were heated to 130 °C in an oven-dried under vacuum prior to use. The autoclave was placed under 40 bar CO_2 pressure and heated to 80 °C. CO_2 of purity grade 4.5 was purchased from Westfalen AG and was applied in all experiments. The epoxide was freshly dried over CaH_2 and distilled prior to use. Catalyst (0.025−0.05 mmol) was transferred into an autoclave followed by addition of 300 equiv of PO. The reactor was closed, pressurized to 40 bar with CO_2, and heated to 80 °C for 20 h. After cooling the reaction vessel to about 0 °C, CO_2 was slowly released. The viscous reaction mixture was diluted with CH_2Cl_2 and transferred to acidified (HCl) methanol. Immediately, polycarbonate precipitated. The mixture was then stirred for several hours and isolated polycarbonate was dried under vacuum at 60 °C. ^{1}H NMR measurement was done from the crude reaction mixture to determine the ratio of cyclic propylene carbonate and poly(propylene carbonate) products. All isolated polycarbonates were analyzed by ^{1}H NMR, where protons adjacent to carbonate linkages show a signal at 4.6 ppm and the content of polyether linkages was verified by the signals at 3.5 ppm.

Table 1. Propylene Oxide (PO)/CO_2 Copolymerization Results[a] with Ball-Milled Zinc Dicarboxylates

entry	catalyst	TON[b]	TOF[c]	% PPC[d]	M_n[e]	M_w/M_n[e]
1	ZnSA[f]	374	19	82	12	12.4
2	ZnGA[f]	1160	58	94	54	4.6
3	ZnAA[f]	867	43	94	38	4.8
4	ZnPA[f]	1107	55	95	52	4.1
5	ZnSA[g]	600	30	83	33	11.1
6	ZnGA[g]	7146	357	96	103	2.8
7	ZnAA[g]	6431	322	96	82	3.2
8	ZnPA[g]	4264	213	95	78	3.4

[a] Polymerization conditions: 0.5 mmol cat, 150 mmol PO, 80 °C, 20 h, 40 bar CO_2 (initial pressure), 500 rpm. [b] Turnover number in grams of polymer per moles of zinc. [c] Turnover frequency in grams of polymer per moles of zinc per hour. [d] Estimated by ^{1}H NMR spectroscopy. [e] Determined by GPC, calibrated with polystyrene standard in THF, M_n given in kg/mol. [f] Not activated. [g] Activated.

Theoretical Calculations. Quantum chemical studies were performed at the BP86[58−60] /SV(P)[61] level of theory, employing the solvation model COSMO.[62] (with a dielectric constant of infinity). For the sake of simplicity and the general character of conclusion, as a model for the polymer, a methyl group was used. As an epoxide for copolymerizaion, ethylene oxide was chosen, and a dimethyl β-ketiminato ligand was used to simulate this class of ligands. For the scan of activation barriers with respect to internuclear distances, the reaction coordinate (OCO) was kept fixed at the values computed for an intermetallic distance of 3.5 Å. Additionally, it was also necessary in the case of the alkoxide intermediate for the model catalyst $[Cu_2]^+$ to keep the C−H bond distances fixed (at around 1.10 Å) in order to avoid a C−H agostic stabilization for longer metal−metal distances that would markedly bias activation barriers.

RESULTS AND DISCUSSION

Experimental Investigation. The lacking knowledge about polymerization mechanisms on heterogeneous zinc dicarboxylates prompted us to investigate not only the already characterized solid state structure of zinc glutarate (ZnGA) and zinc succinate (ZnSA), but also of their higher homologues zinc adipate (ZnAA) and zinc pimelate (ZnPA). To get decent crystals for a structure determination, we used the synthetic route via hydrothermal treatment. For this purpose, the

Table 2. Propylene Oxide (PO)/CO_2 Copolymerization Results[a] with Different Ball-Milling Times of Zinc Glutarate

entry	time of BM	TON[b]	TOF[c]	% PPC[d]	M_n[e]	M_w/M_n[e]
1	0 min	0	0	/	/	/
2	10 min[f]	1080	54	94	48	3.7
3	30 min[f]	1548	77	93	23	4.4
4	1 h[f]	1432	72	93	18	8.2
5	2 h[f]	1348	67	92	13	5.9
6	4 h[f]	2108	105	94	43	4.9
7	10 min[g]	1056	53	94	24	4.3
8	30 min[g]	1416	71	94	43	4.6
9	1 h[g]	1744	87	93	23	6.3
10	2 h[g]	2932	147	95	45	4.0
11	4 h[g]	7146	357	96	103	2.8
12	standard	5876	294	95	72	4.5

[a] Polymerization conditions: 0.5 mmol cat, 150 mmol PO, 80 °C, 20 h, 40 bar, 500 rpm. [b] Turnover number in grams of polymer per moles of zinc. [c] Turnover frequency in grams of polymer per moles of zinc per hour. [d] Estimated by ^{1}H NMR spectroscopy. [e] Determined by GPC, calibrated with polystyrene standard in THF, M_n given in kg/mol. [f] Not activated. [g] Activated.

corresponding zinc nitrate, together with dicarboxylic acid and water, is introduced into a glass-autoclave and heated to 180 °C. After several hours at this temperature, the glass vessel is interstratified with streaks that eventually form the crystalline particles after 1−30 days, depending on the dicarboxylic acid used.

Even though this procedure generally suffers from low yields, highly crystalline particles can be gathered in all cases. Several of these crystals were collected for structure determination; the rest was ground for 4 h via a ball-mill in an inert argon atmosphere.

To minimize abrasion during the grinding procedure, an abrasion resistant ZrO_2-beaker and ZrO_2-balls were used. The received powder was immediately transferred to a glovebox and the correspondent amount of the received powder weighed for CO_2/PO copolymerization experiments (Table 1, entries 1−4). However, very low activities were achieved with this material.

We suppose this inefficiency of the ball-milled zinc dicarboxylates to result from inactive Zn-species on the newly generated surface. As the treatment was conducted in an inert argon atmosphere, no water molecules or other reagents could react with the Zn-species on the newly created faces. However post-treatment of the material with water and thorough drying in a vacuum-oven at 130 °C (to anticipate any chain transfer reaction with residual water) allowed us to activate the material. Indeed, the post-modified material shows a largely increased activity toward PO/CO_2 copolymerization (Table 1, entries 5−8). We ascribe this effect to the generation of ZnOH-groups on the surface, which then show an activity for the polymerization.

To further determine the effect of grinding and post-activation, we investigated a series of different ball-milling intervals with the system ZnGA. In this series, the crystalline ZnGA particles from the hydrothermal synthesis were ball-milled for 10 min, 30 min, 1 h, 2 h, and 4 h, respectively, in an inert argon atmosphere and copolymerization experiments conducted with the resulting materials (Table 2, entries 2−6). Copolymerization experiments with the untreated ZnGA yielded no product at all; the material obtained via hydrothermal synthesis route is constituted of big crystals with almost no surface area (Table 2, entry 1).

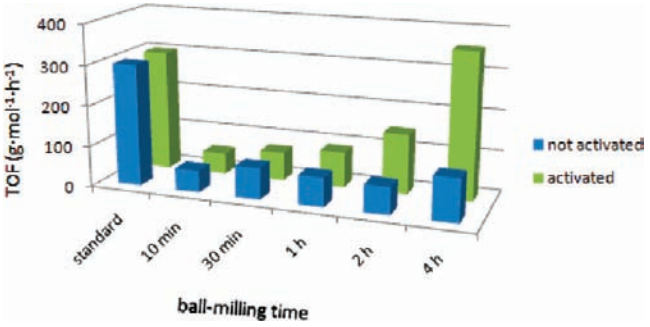

Figure 1. Graphical presentation of the correlation between ball-milling time, activity, and the influence of post-activation.

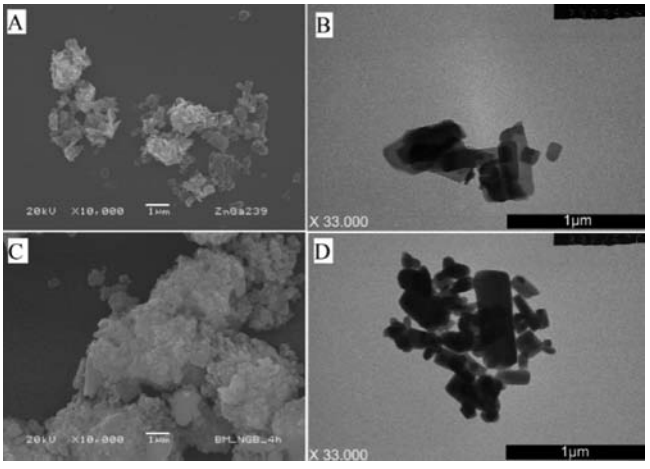

Figure 2. High-resolution SEM- and TEM-images of standard ZnGA (A and B) and ball-milled ZnGA (ball-milling interval: 4 h) (C and D).

Additionally, the ground material was post-activated the same way as previously described with water, then thoroughly dried and used in copolymerization (Table 2, entries 7−11). For a better comparison, a copolymerization experiment with standard ZnGA (from ZnO and glutaric acid) was realized using the same conditions (Table 2, entry 12). The activity of ZnGA formed via standard procedure corresponds with TOF ≈ 300 h^{-1} to that of ZnGA currently reported in literature.[42,49,50,63,64]

Ball-milling of ZnGA without post-activation leads to almost no improvement in activity. Nonactivated material shows the same efficiency for copolymerization, independent of the previous grinding interval, which can be attributed to the lack of initiator groups on the surface. Again, post-activation with water leads to active material which shows the expected correlation of grinding time and activity. For a better comparison, a graphical presentation of the activities in Table 2 is given in Figure 1.

From the activity data given in Table 1, it is apparent that all zinc dicarboxylates except ZnSA show a comparable activity for PO/CO_2 copolymerization. Indeed, ZnGA, ZnAA, and ZnPA exhibit a comparable efficiency in their activated (TOF ≈ 300 h^{-1}) as well as in their nonactivated state (TOF ≈ 50 h^{-1}). However, the activity of the ball-milled (TOF = 19 h^{-1}) and post-activated ZnSA (TOF = 30 h^{-1}) does not change to the same degree as for ZnGA and its higher homologues.

Comparison of Surface Area and Particle Size. To further investigate the correlation between grinding and activity, the surface area of the ball-milled samples and the reference

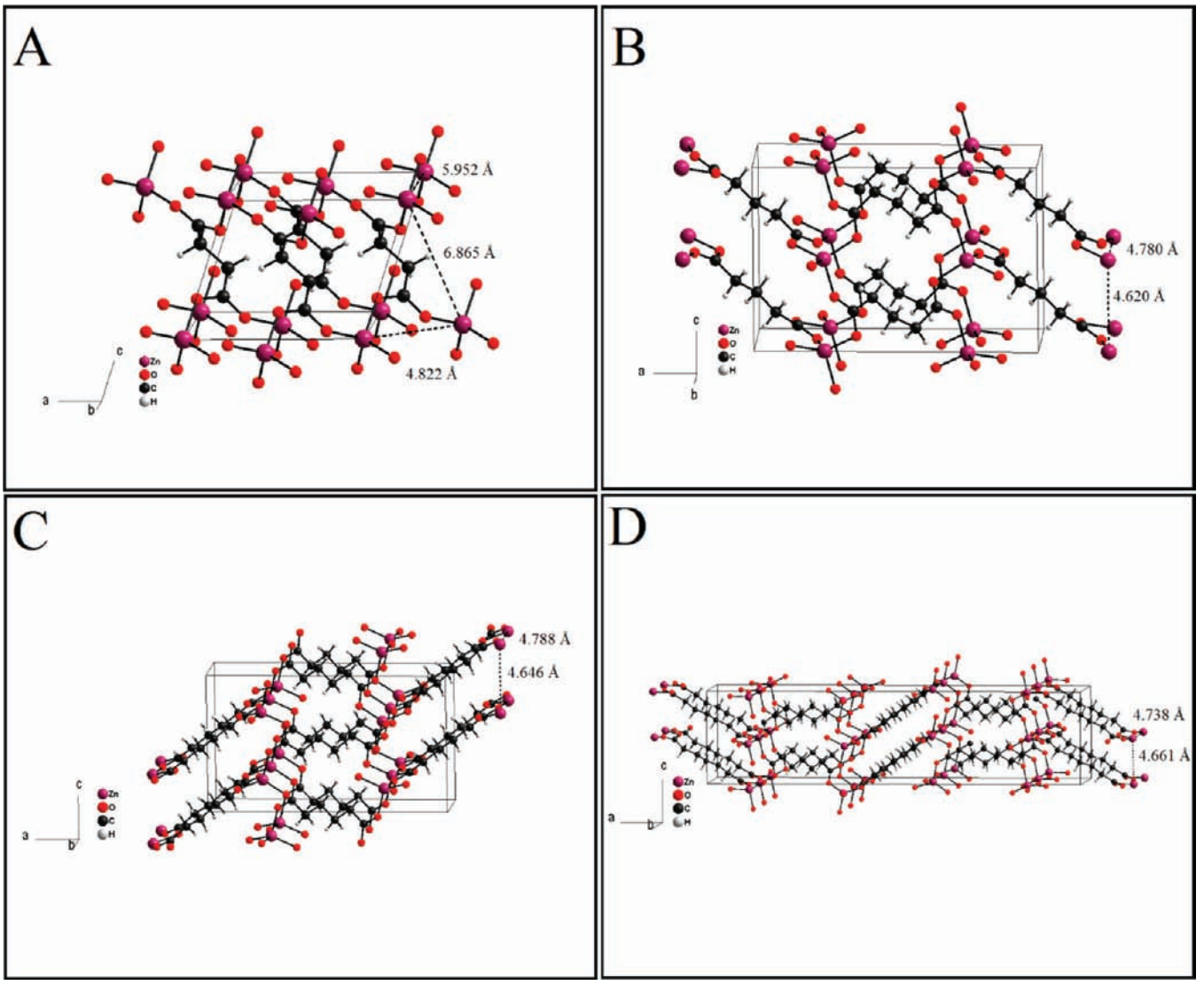

Figure 3. Solid state structures of (A) ZnSA,[56,57] (B) ZnGA,[40,41] (C) ZnAA, and (D) ZnPA (Diamond drawing).

(standard) sample was determined via BET-measurements (N_2) and the particle sizes compared in high-resolution SEM- and TEM-images.

The ZnGA synthesized via standard procedure has a surface area of 15.2 m^2/g; the samples that were ball-milled for 4 h show a surface area of 8.9 m^2/g (ZnSA), 14.9 m^2/g (ZnGA), 9.6 m^2/g (ZnAA), and 8.5 m^2/g (ZnPA), respectively. These results show that all materials have a surface area of approximately 10−15 m^2/g and no microporosity at all, confirming that the copolymerization only takes place on the outer surface of zinc carboxylate. As the surface area of all four catalysts lies in the same range, it cannot be the decisive factor for the activity difference between ZnSA and its higher homologues.

Additionally, high-resolution SEM- and TEM-images of the material were taken (Figure 2). This allowed us to compare the morphology and particle size of the resulting materials. The TEM-images indicate that the ball-milling of the crystalline particles for 4 h delivers ZnGA platelets with approximately the same particle size (and therefore surface area and activity, Table 2, entry 11) as for the material synthesized with the standard procedure (Table 2, entry 12).

Further ball-milling would presumably only show a marginal effect on activity, as the particle size of the resulting material after 4 h of ball-milling is already situated at the lower end (<1 μm) of what ball-mills are capable to treat. As a side note, this observation also provides insight as to why logical modifications of the zinc dicarboxylates only lead to a marginal effect in its efficiency.

All strategies investigated so far to increase the activity were based on the increase of its surface area (stirring procedure, post-modification, additives, growth controllers). It becomes obvious that all of these strategies are restricted due to the limitations in further downsizing the material.

In conclusion, the surface area, the particle size, and the morphology of ZnSA (Figure S1 in Supporting Information) are comparable to those of ZnGA. The reason for the activity difference between ZnSA and its higher homologues must therefore be attributed to a different solid state structure of ZnSA, which does not provide the active surface species that are necessary for copolymerization.

Comparison of Solid State Structures. To gain better insight into the effect of the surface constitution, the solid state structures of the different zinc dicarboxylates have to be compared. In two

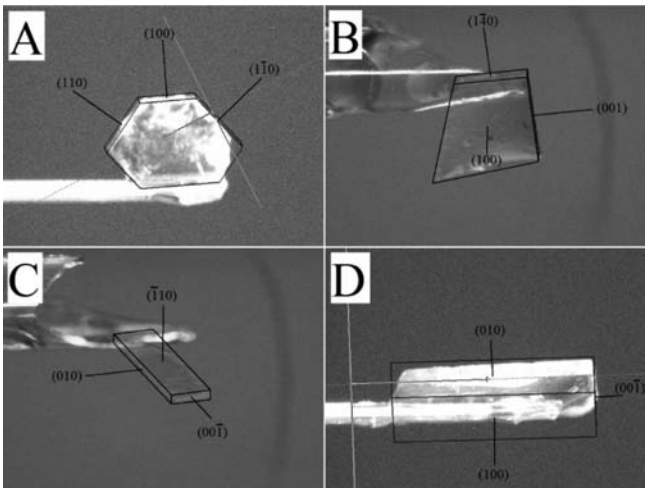

Figure 4. Orientation and growth direction of crystals (A) ZnSA, (B) ZnGA, (C) ZnAA, and (D) ZnPA.

independent attempts, the molecular structure of ZnSA has been reported.[56,57] Considerable variations in the solid state structure of ZnSA are observed, which presumably arises from the different synthetic conditions employed. However, in our hands, only the synthesis of the monoclinic C2-symmetric structure of ZnSA could be achieved (Figure 3A). The solid state structure of ZnGA has been verified as described in literature (Figure 3B). The two structures of ZnSA and ZnGA vary considerably, which makes a clear statement about the active species difficult. To obtain complete insight into the inefficiency of ZnSA compared to the other zinc dicarboxylates, we also determined the solid state structure of ZnAA and ZnPA (Figure 3C,D). The crystalline particles for structure determination were taken from the hydrothermal synthesis route and their orientation and growth direction were determined (Figure 4).

As expected, ZnGA, ZnAA, and ZnPA show the same space group $P2/c$ and a very similar structure, with the cell axes a and c and all angles having approximately the same axes lengths (degrees). Only the cell axis b differs considerably in each structure, due to the elongated C-backbone of the higher dicarboxylic acid, which results in a drawn-out unit cell. Most strikingly, the constitution of the hkl-plane [100] remains completely the same in all three structures (ZnGA, ZnAA, and ZnPA), with four Zn-atoms in a very defined spatial conformation and a Zn−Zn distance of 4.6−4.8 Å (Figure 5). This structural motif however cannot be found in the solid state structure of ZnSA, which could explain the activity difference between ZnSA and its higher homologues, when a bimetallic mechanism is assumed. The distance of 4.6−4.8 Å is also situated in the same area as for regular dinuclear homogeneous complexes that are used in CO_2/epoxide copolymerization and is therefore considered as necessary for any bimetallic mechanism on a heterogeneous zinc dicarboxylate surface.

When the structures of ZnGA, ZnAA, and ZnPA are compared to ZnSA (Figure 5A), it becomes apparent why this material is much less active than its higher homologues. For an active ZnSA catalyst, the [001] plane needs to have the largest expansion, as on most other [hkl] planes, no Zn−Zn couples can be found (compare Figures S3 and S4 for views along b- and c-axes). Such a directional growth is rather difficult, which limits the efficiency of ZnSA. When ZnSA is treated with a ball-mill, the breaking events will only expose few new surfaces with the necessary Zn−Zn couples.

ZnGA, ZnAA and ZnPA crystals, however, can be grown or cut in any direction and still have exposed Zn−Zn couples in the right spatial conformation. This means that, for example, breaking the ZnGA along its [100], [010], or [001] plane will always lead to newly exposed Zn−Zn couples with an intermetallic distance of 4.6−4.8 Å. For a better comparison, some more selected Zn−Zn distances on several important [hkl] planes are given for all four treated zinc dicarboxylates (Table S1 in Supporting Information). From a statistical point of view, during ball-milling, ZnGA, ZnAA, and ZnPA will be activated to a much larger extend than ZnSA, which explains the polymerization data given in Table 1. A close-up view onto the relevant structure motif in zinc glutarate with the highlighted Zn−Zn distances is given in Figure 6.

This is the first time that a bimetallic CO_2/epoxide copolymerization mechanism has been suggested for a heterogeneous catalyst. However, it is not clear yet which intermetallic distance shows an optimum toward copolymerization efficiency and/or selectivity. To further investigate the influence of the intermetallic distance, theoretical calculations were conducted. These will also allow to substantiate the conclusions derived in the experimental part and to corroborate the necessity of two closely linked active metal centers on the surface of heterogeneous zinc dicarboxylates, as well as in homogeneous systems.

Theoretical Investigation. The activity of a catalyst in the copolymerization of CO_2 and epoxides depends on the activation barrier that has to be overcome. This activation barrier can be defined as the difference between the energetically most favorable species (the catalyst resting state) and the typically rate-limiting epoxide ring-opening transition state. However, as other reactions compete with the copolymerization and the desired polycarbonate formation, simultaneously, the corresponding activation barriers of these side reactions need to be as high as possible for an efficient and selective catalyst. Such side reactions are in particular epoxide homopolymerization and formation of cyclic carbonates.

For PPC catalysts, it can be expected that the major parameters that influence the activation barrier of the main and side reactions are the electrophilicity of the metal centers and the metal−metal distance. As in both side and main reactions, the oxidation states of the reactants and the catalytic centers do not change, general and rather metal independent relations can be assumed to define an optimal distance between two metal sites, for example, with respect to catalyst activity. An attempt to substantiate this idea was tried in the following via quantum chemical calculations.

To scan the influence of intermetallic distances d_{MM}, it is necessary to be able to perform computations over a wide range of d_{MM}, which is only possible with a model catalyst. The activation barriers E_a, which are obtained by a comparison of energies E of the resting states and the rate-limiting transition states of the main or the side reaction, are given by

$$E_a(d_{MM}) = E^{TS}(d_{MM}) - E^{RS}(d_{MM})$$

It was assumed here that the actually relevant *Gibbs free energy* curves exhibit a similar behavior as the corresponding pure energy curves given in the following. A critical point in this concept is that it is not trivial to choose a model catalyst that offers a reasonable description of the real zinc carboxylate

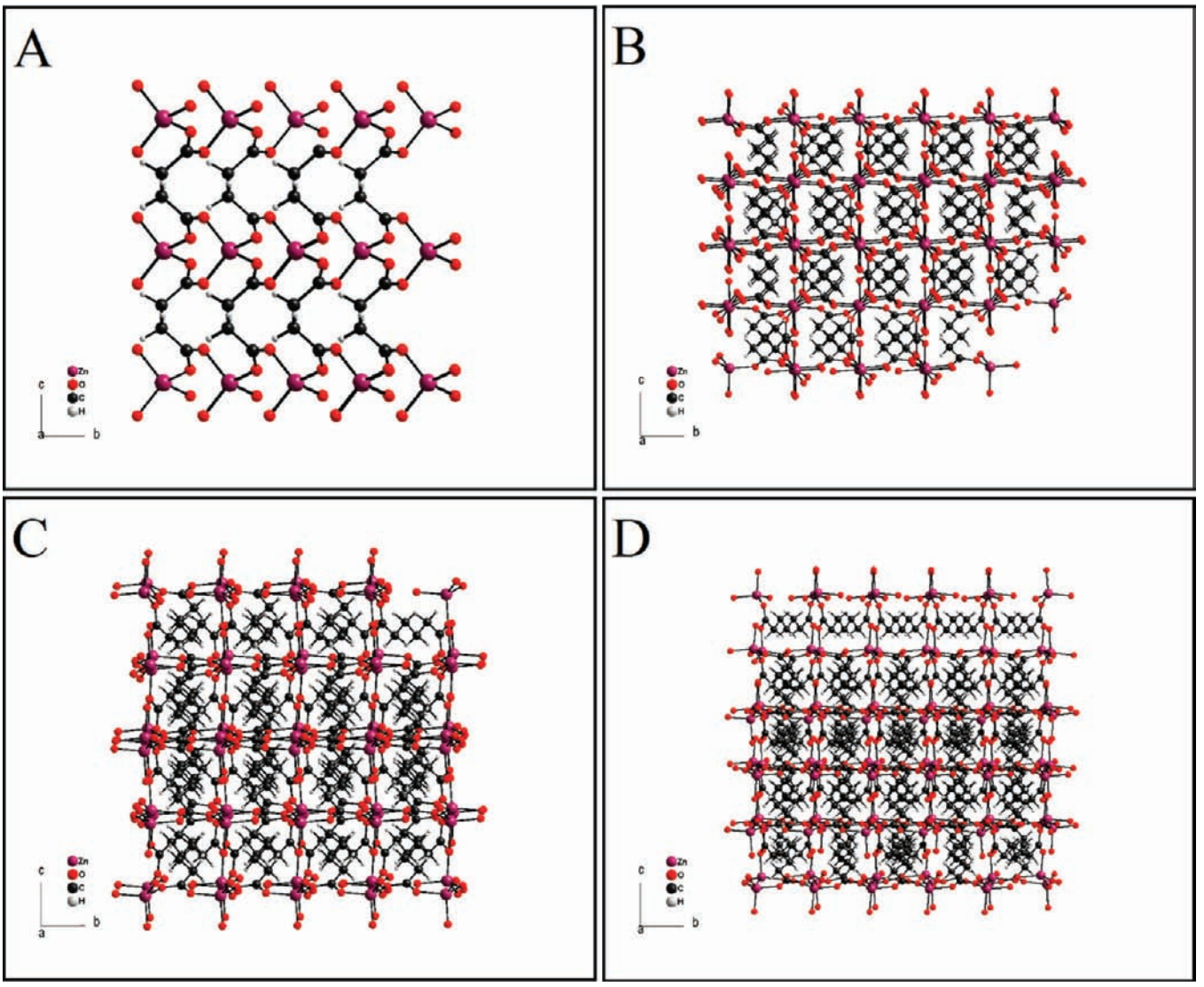

Figure 5. View along *a*-axis of (A) ZnSA,[56,57] (B) ZnGA,[40,41] (C) ZnAA, (D) and ZnPA.

systems and at the same time exhibits the flexibility to vary d_{MM} over a sufficiently large range. Real, well-designed catalysts with a restricted metal−metal distance around a well-defined value can eventually corroborate these results.

Therefore, a number of different model catalysts were studied in order to provide a sound basis for the conclusions derived here. A general feature of the dinuclear sites in zinc carboxylate catalysts is that two neighboring metal centers are connected by one carboxylate bridge. Via this bridge, a (formally) constant charge is maintained on both reactant and product side and for both Zn atoms involved in the ring-opening processes (Figure 7).

This feature was implemented in several model catalysts by incorporating either a chloride or an acetate as anionic bridging ligand. In the case of an acetate bridge (which is closest to the real system investigated), the system switches between an exo- and an endo-conformation depending on the metal−metal distance (Figure 8). This disadvantage can be avoided by introducing a chloride bridge, which is more far away from the real structure, but allows to obtain smooth potential curves at the points where in either the reactants or the transition states the bridging carboxylate ligand would jump (typically spontaneously) to the new conformation.

Besides the bridging unit, there are also multiple choices for the remaining ligands, required to coordinatively saturate the metal centers. Whereas the model ligands closest to the real system would be carboxylates, other monoanionic chelating ligands like β-diiminates (BDI) offer the advantage of larger and more favorable angles when bidentately coordinating to *one* metal center (for the two four-coordinate Zn atoms of the considered model catalysts as well as in the heterogeneous Zn dicarboxylates, angles close to the tetrahedron angle of 109° should be preferred). Furthermore, for BDI ligands, there is a reduced tendency to rearrange to multiply bridged structures at shorter metal−metal distances which occurred for terminal carboxylate ligands at 2.5 Å. Apart from this, carboxylates that coordinate with both carboxylic oxygens to the same zinc atom are also avoided in the bulk structures of zinc dicarboxylates due to the high ring tension.

From the considerations above, four model catalyst systems can be derived: $(BDI)_2Zn_2(\mu\text{-Cl})$, $(AcO)_2Zn_2(\mu\text{-Cl})$, $(BDI)_2Zn_2(\mu\text{-AcO})$, and $(AcO)_2Zn_2(\mu\text{-AcO})$. Of these four systems, the $(BDI)_2Zn_2(\mu\text{-AcO})$ model catalyst is the closest to real catalysts described by Coates, that were already presented in the

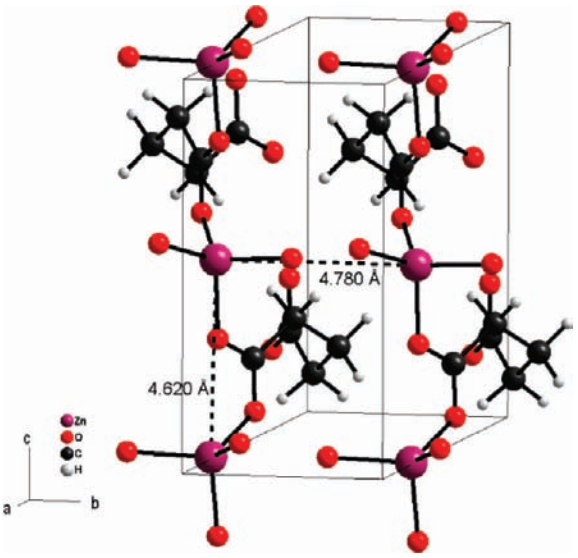

Figure 6. Close-up view of metal distances in zinc glutarate (Zn−Zn distance = 4.6−4.8 Å).

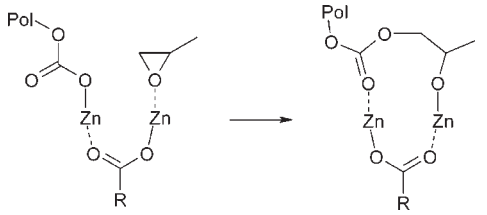

Figure 7. Neighboring neutral zinc centers connected via a carboxylate bridge maintain their charge upon epoxide ring-opening.

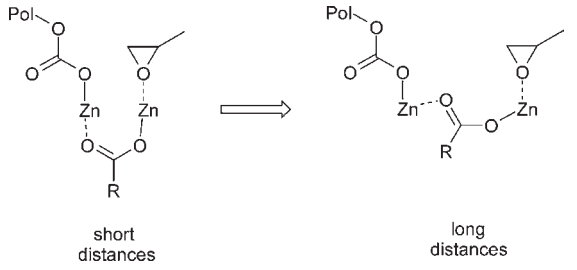

Figure 8. Formation of a new bridging conformation.

introduction. The structural parameters of the transition states for homo- and copolymerization (Figure 9) as well as the computed activation barriers are given in Table 3 for metal−metal distances of 2.5, 3.5, and 4.5 Å (as far as it is possible to obtain reasonable reactant and transition state structures).

The energetics show drastic variations depending on the model catalyst. This mainly reflects the binding strengths of the alkoxide ligand in the precursor. This alkoxide ligand may also be the bridging unit between two metal atoms at shorter distances. However, structural parameters of the transition states are rather similar. The O(nucleophile)−C(epoxy) distance is found to be around 2.1 Å (i.e., a factor of 1.5 larger than typical C−O single bond distances), whereas for the disappearing C(epoxy)−O(epoxy), bond values are situated around 1.8 Å (a factor of 1.3 with respect to C−O single bonds).

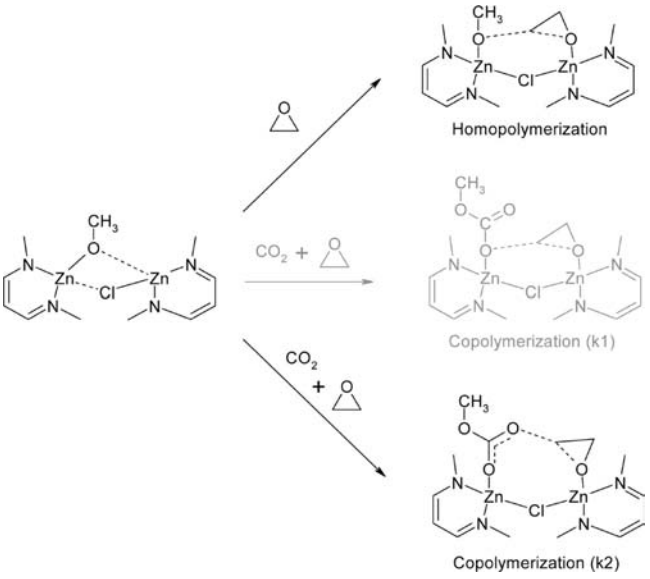

Figure 9. Transition states for simplified models to study Zn−Zn distance dependence of homo- and copolymerization. In Table 3, copolymerization always refers to the κ^2-case, which was found to be generally favored with respect to κ^1. Shown here is the system with a chloride bridge and two β-diiminate ligands.

For all catalyst systems, it can be observed that copolymerization requires lower activation barriers than homopolymerization. This depends partially on the choice of reference resting states: for both homo- and copolymerization, the same alkoxide species is considered. This means that the copolymerization barriers also reflect the typically exothermic and fast (i.e, not rate limiting) reaction between alkoxides and CO_2. The question if alkoxide or carbonate complexes represent the resting state actually depends on both (model) catalyst system as well as process conditions (temperature, CO_2 pressure), but is irrelevant if the focus lies on relative differences between reactive pathways, that is, on catalyst selectivities.

However, with the four dinuclear Zn model catalysts in Table 3, it is only possible to scan distances lower or around those found for bulk structures of heterogeneous Zn dicarboxylates. At larger distances, chloride ligands are not able to bridge anymore, whereas carboxylate bridges tend to drastically interfere with reacting nucleophile and epoxide in the transition state structures, as both the ligand bridge and the actual reacting species strongly prefer to reside as much as possible between the two Zn atoms. Therefore, an alternative model catalyst was chosen that allows (in principle) to model any metal−metal distance. Two Cu^+ atoms without further ligands were chosen. In this case, overall, a monocationic catalyst results, in which every metal center exhibits the d^{10} electronic configuration, which is also characteristic for Zn^{2+} species. Upon ring-opening, the negative counter charge migrates from one side of the dinuclear Cu system to the other side, which however still means no energetic bias (as would be the case if four nonbridging monoanionic ligands, among which would also be the propagating polymer chain, were distributed, for example, as 2 + 2 in the reactant and thus as 3 + 1 in the product). From the results (also in Table 3), it can be concluded that structural parameters are very similar to the dinuclear Zn complexes. As can be seen, for this model catalyst, it was possible to extend metal−metal distances to 5.5 Å and beyond.

Table 3. Dependence of Computed Structural Parameters and Activation Barriers for Homo- And Copolymerization on Metal−metal-Distances[a]

	TS (homopolymerization)			TS (copolymerization)		
d_{MM} [Å]	$d(O^1-C)$ [Å]	$d(C-O^2)$ [Å]	E_a [kJ/mol]	$d(O^1-C)$ [Å]	$d(C-O^2)$ [Å]	E_a [kJ/mol]
			$(BDI)_2Zn_2(\mu\text{-Cl})$			
2.5	2.29	1.99	+235.1	2.14	1.80	+117.6
3.5	2.18	1.78	+132.2	2.07	1.80	+47.5
4.5	2.21	1.75	-	2.08	1.83	-
			$(AcO)_2Zn_2(\mu\text{-Cl})$			
2.5	-	-	-	-	-	-
3.5	2.23	1.78	+66.8	2.11	1.81	−8.3
4.5	2.22	1.77	-	2.11	1.82	-
			$(BDI)_2Zn_2(\mu\text{-AcO})$			
2.5	2.23	1.94	+257.8	2.09	1.84	+102.7
3.5	2.17	1.76	+197.3	2.06	1.81	+102.6
4.5	2.20	1.73	6.7	2.04	1.85	−50.1
			$(AcO)_2Zn_2(\mu\text{-AcO})$			
2.5	-	-	-	-	-	-
3.5	-	-	-	-	-	-
4.5	2.22	1.74	−46.6	2.08	1.84	−96.9
			$(Cu^+)_2$			
2.5	2.33	1.97	+119.9	2.21	1.77	+40.3
3.5	2.25	1.80	+92.7	2.15	1.78	+27.6
4.5	2.25	1.71	−16.9	2.10	1.82	−58.6
5.5	2.24	1.71	−54.6	2.16	1.81	−97.0

[a] O^1 denotes O of the attacking nucleophile (alkoxide or carbonate) and O^2 represents the former epoxy O atom.

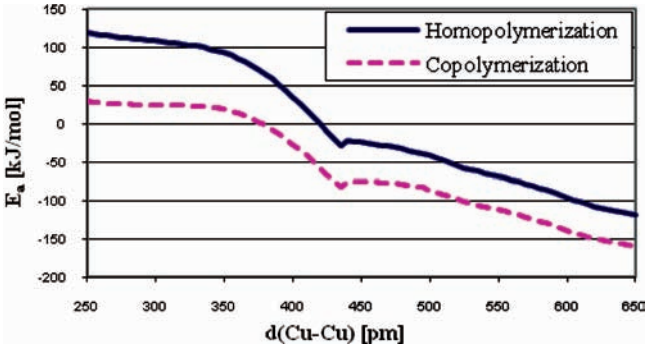

Figure 10. Variation of activation barriers of homo- and copolymerization with metal−metal distance, computed for a very simplified catalyst consisting of two Cu^+ ions.

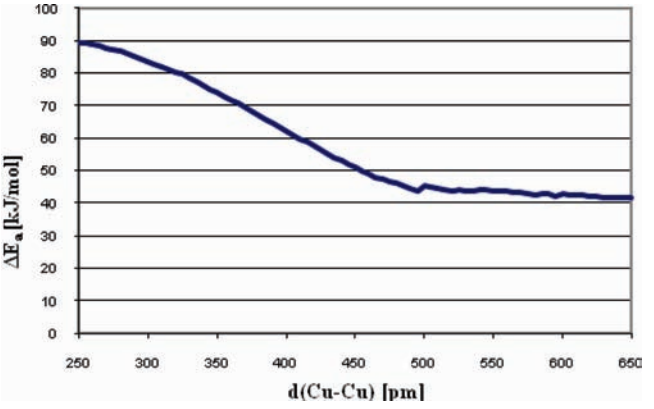

Figure 11. Metal−metal distance dependent difference of activation barriers of homo- and copolymerization, computed for a very simplified catalyst consisting of two Cu^+ ions.

For the dinuclear Cu model catalyst, an energetic scan with an increment of 0.05 Å was performed for homo- and copolymerization. Graphical representations of homopolymerization and copolymerization barriers as well as of the resulting energetic differences between these two reactions, are given in Figures 10 and 11, respectively.

For dinuclear Zn complexes, the activation barrier of copolymerization (and generally of all ring-opening reactions) is lowered upon increasing the metal−metal distance. This can partially be explained by the weaker binding of the alkoxide precursor to the two Cu^+ cations. Above 4.35 Å, the methoxide actually "chooses" one Cu^+ and the bridge becomes unsymmetrical; for metal−metal distances below this value, the activation barrier for epoxide ring-opening increases steeply upon lowering d_{MM}. Another important point represents the intrinsic barrier of epoxide ring-opening by a nucleophile. For an S_N2 like reaction, a linear orientation of O−C−O would be desirable in the transition state. Indeed, part of the lowering of activation barriers for ring-opening can be traced back to O−C−O angles being able to come closer to 180° at larger metal−metal distances. This effect

dx.doi.org/10.1021/ja204481w |J. Am. Chem. Soc. 2011, 133, 13151–13161

becomes even more pronounced for homopolymerization than for copolymerization, as in homopolymerization all three atoms between the two metal centers should assume a linear arrangement, whereas in κ^2-copolymerization, at least five atoms take part and thus a higher structural flexibility is possible. Therefore, at short metal−metal distances, homopolymerization is more strongly disfavored with respect to copolymerization, whereas at larger metal−metal distances, the two competing reactions become closer in energy (Figure 11).

Thus for larger distances, most significantly up to 430 pm, catalytic activity becomes higher, whereas smaller distances below 500 pm offer the advantage to better suppress homopolymerization.

In conclusion, the optimal Zn−Zn distance for copolymerization of epoxides and CO_2 should be located between 4.3 and 5.0 Å. The common distance found in zinc dicarboxylates of 4.6−4.8 Å probably leads to a balanced optimum between activity and selectivity. At higher metal−metal distances, homopolymerization and backbiting (which is not discussed here) become more probable, increasing the side product formation. Therefore, also for homogeneous complexes, the Zn−Zn distance has to be carefully adjusted to a certain range and cannot be chosen deliberately.

To our knowledge, this is the first time that the effect of the intermetallic distance on CO_2/epoxide copolymerization has been discussed and calculated. The theoretical investigation corroborates that two cooperating metal centers are necessary for any activity in heterogeneous zinc dicarboxylates. In other words, the more Zn−Zn couples that can be found on the surface, the higher the activity of the catalyst will be. In accordance to this, ZnSA will show a reduced activity than its higher homologues as the occurrence of Zn−Zn couples is lower in this catalyst. The effect of intermetallic distance can be extended to homogeneous systems that assume a bimetallic copolymerization pathway.

CONCLUSION

We designed a synthesis procedure which allows comparison of all four zinc dicarboxylates (ZnSA, ZnGA, ZnAA, and ZnPA) and their efficiency in CO_2/PO copolymerization. Through careful handling in an inert atmosphere, we were able to prove that the material needs to be activated in order to generate initiator groups on the surface that are able to copolymerize.

From the copolymerization experiments conducted, the activity discrepancy between ZnSA and its higher homologues becomes obvious. As this difference can neither be attributed to the surface areas nor to the particle sizes, it can be concluded that the molecular structure is the decisive factor. The major difference between ZnSA and its higher homologues is the occurrence of Zn−Zn surface couples in a well-defined spatial distance between 4.6 and 4.8 Å.

The importance of two closely linked metal sites has already been described for homogeneous complexes in literature. Furthermore, theoretical calculations conducted in this work to identify an "ideal" Zn−Zn distance suggest an optimal separation of Zn atoms in the range of 4.3−5.0 Å, which gives a balanced optimum between activation energy and selectivity toward copolymerization

The combined experimental and theoretical results allow a more complete understanding of the surface processes on zinc dicarboxylates. A well-defined spatial distance and the activation of the surface metal sites is essential to give a catalytically active material. These results strongly indicate that, for heterogeneous zinc dicarboxylates, a bimetallic mechanism is at work on the surface.

However, the activities with such catalysts are restricted due to a restrained surface and diffusion limitations. Furthermore, grinding of the material improves its efficiency as expected, even though the increase is strongly limited due to limitations in further downsizing the material. New strategies should therefore focus on introduction of two metallic species into a molecular framework that does not comprise bulky material, in which no catalysis can take place. Therefore, new strategies have to focus on homogeneous systems that comprise two metal centers or a cooperative binary linked ligand system.

ASSOCIATED CONTENT

Supporting Information. Single crystal X-ray structure determination data of compound ZnAA; Zn−Zn distances on [hkl] faces, views along *b*- and *c*-axes and PXRD data of different zinc dicarboxylates; complete ref 9. This material is available free of charge via the Internet at http://pubs.acs.org.

AUTHOR INFORMATION

Corresponding Author
rieger@tum.de

ACKNOWLEDGMENT

The financial support of the BMBF (grant 01 RC 0902 A) is gratefully acknowledged. Thanks to Dr. Marianne Hanzlik for TEM- and SEM-images and to Dr. Xaver Hecht for BET-measurements.

REFERENCES

(1) Gerngross, T. U.; Slater, S. C. *Sci. Am.* **2000**, *283*, 37.
(2) Gross, R. A.; Kalra, B. *Science* **2002**, *297*, 803.
(3) Okada, M. *Prog. Polym. Sci.* **2001**, *27*, 87.
(4) Danner, H.; Braun, R. *Chem. Soc. Rev.* **1999**, *28*, 395.
(5) Santer, B. D.; Taylor, K. E.; Wigley, T. M. L.; Johns, T. C.; Jones, P. D.; Karoly, D. J.; Mitchell, J. F. B.; Oort, A. H.; Penner, J. E.; Ramaswamy, V.; Schwarzkopf, M. D.; Stouffer, R. J.; Tett, S. *Nature* **1996**, *382*, 39.
(6) Broecker, W. S. *Science* **1997**, *278*, 1582.
(7) Meehl, G. A.; Washington, W. M. *Nature* **1996**, *382*, 56.
(8) Kacholia, K.; Reck, R. A. *Clim. Change* **1997**, *35*, 53.
(9) Arakawa, H.; et al. *Chem. Rev.* **2001**, *101*, 953.
(10) Cooper, A. I. *J. Mat. Chem.* **2000**, *10*, 207.
(11) Bolm, C.; Beckmann, O.; Dabard, O. A. G. *Angew. Chem., Int. Ed.* **1999**, *38*, 907.
(12) Dittmeyer, R.; Keim, W.; Kreysa, G.; Oberholz, A. *Winnacker-Küchler: Chem. Tech.* **2005**, *4*.
(13) Inoue, S.; Koinuma, H.; Tsuruta, T. *Makromol. Chem.* **1969**, *130*, 210.
(14) Kroeger, M.; Folli, C.; Walter, O.; Doering, M. *Adv. Synth. Catal.* **2005**, *347*, 1325.
(15) Allen, S. D.; Moore, D. R.; Lobkovsky, E. B.; Coates, G. W. *J. Am. Chem. Soc.* **2002**, *124*, 14284.
(16) Kroeger, M.; Doering, M. *Catal. Today* **2006**, *115*, 146.
(17) Lee, B. Y.; Kwon, H. Y.; Lee, S. Y.; Na, S. J.; Han, S.; Yun, H.; Lee, H.; Park, Y.-W. *J. Am. Chem. Soc.* **2005**, *127*, 3031.
(18) van Meerendonk, W. J.; Duchateau, R.; Koning, C. E.; Gruter, G.-J. M. *Macromol. Rapid Commun.* **2004**, *25*, 382.
(19) Klaus, S.; Lehenmeier, M. W.; Anderson, Carly E.; Rieger, B. *Coord. Chem. Rev.* **2011**, *25*, 1460.
(20) Darensbourg, D. J. *Chem. Rev.* **2007**, *107*, 2388.
(21) Kember, M. R.; Buchard, A.; Williams, C. K. *Chem. Commun.* **2011**, *47*, 141.

(22) Luinstra, G. A.; Haas, G. R.; Molnar, F.; Bernhart, V.; Eberhardt, R.; Rieger, B. *Chem.—Eur. J.* **2005**, *11*, 6298.
(23) Jacobsen, E. N. *Acc. Chem. Res.* **2000**, *33*, 421.
(24) Nielsen, L. P. C.; Stevenson, C. P.; Blackmond, D. G.; Jacobsen, E. N. *J. Am. Chem. Soc.* **2004**, *126*, 1360.
(25) Hansen, K. B.; Leighton, J. L.; Jacobsen, E. N. *J. Am. Chem. Soc.* **1996**, *118*, 10924.
(26) Cohen, C. T.; Chu, T.; Coates, G. W. *J. Am. Chem. Soc.* **2005**, *127*, 10869.
(27) Darensbourg, D. J.; Yarbrough, J. C. *J. Am. Chem. Soc.* **2002**, *124*, 6335.
(28) Darensbourg, D. J.; Yarbrough, J. C.; Ortiz, C.; Fang, C. C. *J. Am. Chem. Soc.* **2003**, *125*, 7586.
(29) Darensbourg, D. J.; Rodgers, J. L.; Mackiewicz, R. M.; Phelps, A. L. *Catal. Today* **2004**, *98*, 485.
(30) Allen, S. D.; Moore, D. R.; Lobkovsky, E. B.; Coates, G. W. *J. Organomet. Chem.* **2003**, *683*, 137.
(31) Bok, T.; Yun, H.; Lee, B. Y. *Inorg. Chem.* **2006**, *45*, 4228.
(32) Pilz, M. F.; Limberg, C.; Lazarov, B. B.; Hultzsch, K. C.; Ziemer, B. *Organometallics* **2007**, *26*, 3668.
(33) Piesik, D.; Range, S.; Harder, S. *Organometallics* **2008**, *27*, 6178.
(34) Kember, M. R.; Knight, P. D.; Reung, P. T.; Williams, C. K. *Angew. Chem.* **2009**, *121*, 949.
(35) Kember, M. R.; White, A. J. P.; Williams, C. K. *Inorg. Chem.* **2009**, *48*, 9535.
(36) Kember, M. R.; White, A. J. P.; Williams, C. K. *Macromolecules* **2010**, *43*, 2291.
(37) Buchard, A.; Kember, M. R.; Sandeman, K. G.; Williams, C. K. *Chem. Commun.* **2010**, *47*, 212.
(38) Nakano, K.; Hashimotoa, S.; Nozaki, K. *Chem. Sci.* **2010**, *1*, 369.
(39) Vagin, S. I.; Reichardt, R.; Klaus, S.; Rieger, B. *J. Am. Chem. Soc.* **2010**, *132*, 14367.
(40) Zheng, Y. Q.; Lin, J. L.; Zhang, H. L. *Z. Kristallogr.—New Cryst. Struct.* **2000**, *215*, 535.
(41) Kim, J.-S.; Kim, H.; Ree, M. *Chem. Mater.* **2004**, *16*, 2981.
(42) Ree, M.; Hwang, Y.; Kim, J.-S.; Kim, H.; Kim, G.; Kim, H. *Catal. Today* **2006**, *115*, 134.
(43) Meng, Y. Z.; Du, L. C.; Tiong, S. C.; Zhu, Q.; Hay, A. S. *J. Polym. Sci. Part A* **2002**, *40*, 3579.
(44) Ree, M.; Bae, J. Y.; Jung, J. H.; Shin, T. J. *Kor. Polym. J.* **1999**, *7*, 333.
(45) Wang, J. T.; Zhu, Q.; Lu, X. L.; Meng, Y. Z. *Eur. Polym. J.* **2005**, *41*, 1108.
(46) Kim, J.-S.; Kim, H.; Yoon, J.; Heo, K.; Ree, M. *J. Polym. Sci., Part A: Polym. Chem.* **2005**, *43*, 4079.
(47) Wang, S. J.; Du, L. C.; Zhao, X. S.; Meng, Y. Z.; Tjong, S. C. *J. Appl. Polym. Sci.* **2002**, *85*, 2327.
(48) Caroll W. E.; Motika S. A. US Patent 4.960.862 1990.
(49) Ree, M.; Bae, J. Y.; Jung, J. H.; Shin, T. J. *J. Polym. Sci. Part A* **1999**, *37*, 1863.
(50) Kim, J.-S.; Ree, M.; Shin, T. J.; Han, O. H.; Cho, S. J.; Hwang, Y.-T.; Bae, J. Y.; Lee, J. M.; Ryoo, R.; Kim, H. *J. Catal.* **2003**, *218*, 209.
(51) Kim, J. S.; Ree, M.; Lee, S. W.; Oh, W.; Baek, S.; Lee, B.; Shin, T. J.; Kim, K. J.; Kim, B.; Luning, J. *J. Catal.* **2003**, *218*, 386.
(52) Zhu, Q.; Meng, Y. Z.; Tjong, S. C.; Zhang, Y. M.; Wan, W. *Polym. Int.* **2003**, *52*, 799.
(53) Wang, J. T.; Shu, D.; Xiao, M.; Meng, Y. Z. *J. Appl. Polym. Sci.* **2006**, *99*, 200.
(54) Sakharov, A. M.; Il'in, V. V.; Rusak, V. V.; Nysenko, Z. N.; Klimov, S. A. *Russ. Chem. Bull. Int. Ed.* **2002**, *51*, 1451.
(55) Eberhardt, R.; Allmendinger, M.; Zintl, M.; Troll, C.; Luinstra, G. A.; Rieger, B. *Macromol. Chem. Phys.* **2004**, *205*, 42.
(56) Bowden, T. A.; Milton, H. L.; Slawin, A. M. Z.; Lightfoot, P. *Dalton Trans.* **2003**, 936.
(57) Pan, J.; Zhang, G.; Zheng, Y.; Lin, J.; Xu, W. *J. Cryst. Growth* **2007**, *308*, 89.
(58) Becke, A. D. *Phys. Rev. A* **1988**, *38*, 3098.
(59) Perdew, J. *Phys. Rev. B* **1986**, *33*, 8822.
(60) Vosko, S. H.; Wilk, L.; Nusair, M. *Can. J. Phys.* **1980**, *58*, 1200.
(61) Schäfer, A.; Horn, H.; Ahlrichs, R. *J. Chem. Phys.* **1992**, *97*, 2571.
(62) Klamt, A.; Schüürmann, G. *J. Chem. Soc., Perkin Trans 2* **1993**, 799.
(63) Kobayashi, M.; Inoue, S.; Tsuruta, T. *J. Polym. Sci., Polym. Chem. Ed.* **1973**, *11*, 2383.
(64) Soga, K.; Imai, E.; Hattori, I. *Polym. J.* **1981**, *13*, 407.